Quantum phase transitions of multispecies Dirac fermions

H.-M. Guo,[1] Lei Wang,[2] and R. T. Scalettar[3]

[1]*Department of Physics, Key Laboratory of Micro-Nano Measurement-Manipulation and Physics (Ministry of Education), Beihang University, Beijing 100191, China*

[2]*Beijing National Lab for Condensed Matter Physics and Institute of Physics, Chinese Academy of Sciences, Beijing 100190, China*

[3]*Physics Department, University of California, Davis, California 95616, USA*

(Received 8 November 2017; revised manuscript received 8 May 2018; published 28 June 2018)

We use the determinant quantum Monte Carlo method (DQMC) to study the interaction-driven semimetal to antiferromagnetic insulator transition in a π-flux Hamiltonian with modulated hoppings, a model which has two species of Dirac fermions. It is found that the critical interaction strength U_c is decreased by reducing the velocity of the outer Dirac cone, while the inner cone velocity fixes the bandwidth. Although U_c is monotonic, at fixed inverse temperature β the antiferromagnetic (AF) structure factor has a maximum as a function of the hopping modulation. We also study the corresponding strong coupling (Heisenberg model) limit, where the sublattice magnetization is enhanced by the alternation of the exchange couplings. The AF order is shown to be nonmonotonic, and maximal at an intermediate degree of anisotropy, in qualitative agreement with the Hubbard model. These results quantify the effect of the velocities on the critical interaction strength in Dirac fermion systems and enable an additional degree of control which will be useful in studying strong correlation physics in ultracold atoms in optical lattices.

DOI: 10.1103/PhysRevB.97.235152

I. INTRODUCTION

Much recent progress has been made in studying condensed matter emergent quasiparticles which have close analogs in high-energy physics. A primary example is the behavior of electrons on graphene's honeycomb lattice, which are described by two-dimensional (2D) Dirac fermions, and whose unusual physical properties have triggered great interest [1]. Other solutions of the Dirac equation, Majorana fermions (neutral particles that are their own antiparticle) and Weyl fermions, have also been detected in condensed-matter systems [2–4].

These three kinds of fermions have half-integer spin, similar to their high energy analogs, but solid state systems may also have other quasiparticles. Fermions described by a simple $\mathbf{k}\cdot\mathbf{S}$ Hamiltonian with $\mathbf{S}$ the spin operator (obeying the Lie algebra of SU(2)] of spin-1 or spin-3/2 have been reported [5–7]. While these studies focus on three spatial dimensions, realizations similar to graphene in which fermionic quasiparticles are constrained to move in two spatial dimensions, have been considered. The low-energy excitations of itinerate electrons on a Lieb lattice are described by a 2D $\mathbf{k}\cdot\mathbf{S}$ Hamiltonian with pseudospin 1, and have been realized in photonic lattices [8,9] and engineered atomic lattices [10–12]. Generalizations to arbitrary spin S have been obtained in stacked triangular lattices [13] and 2D optical superlattices [14,15].

An important phenomenon exhibited by these fermions is the interaction-driven metal-insulator transition (MIT). Intense research has been carried out on 2D spin-1/2 Dirac fermions in the Hubbard model on a honeycomb lattice and π-flux square lattice, where the simplest scenario of a direct and continuous transition has been confirmed [16–21]. The quantum critical behavior in the vicinity of the phase transition is universal and is described in the continuous limit by the Gross-Neveu model. Studies of spin-1 Dirac fermions have an even longer history. The Lieb lattice hosts such fermions and belongs to a class of bipartite geometries where a rigorous theorem implies a ground state at half-filling with a nonzero spin and long-ranged ferromagnetic order for $U > 0$ [22,23].

It is natural to study the interaction effects in other 2D spin-S Dirac systems. In this paper we consider the MIT and magnetic order in a system similar to that of spin-3/2 Dirac fermions in which a birefringent breakup of the doubly degenerate yields Dirac cones with two different "speeds of light" [24–26]. The velocities of the *normal* spin-3/2 Dirac fermions are fixed to the values proportional to $\frac{3}{2},\frac{1}{2}$, but our realization can continuously tune the velocities of the Dirac cones. The setup can be realized in the π-flux model with modulated hoppings which we solve using DQMC. It is found that the critical interaction scales with the velocity of the outer Dirac cone while the inner cone fixes the bandwidth. The present setup provides an ideal system to study the critical interaction of Dirac fermions with continuously tuned velocity. We also show that in the corresponding Heisenberg model, which is the strong coupling limit of the π-flux Hubbard model, the sublattice magnetization shows a peak as the velocity is decreased, providing an illustration of the interesting phenomenon of enhancing quantum antiferromagnetism by weakening the bonds.

II. MODEL AND METHOD

We start from the π-flux Hubbard model,

$$\hat{\mathcal{H}} = \sum_{\langle ij\rangle\sigma} t_{ij} e^{i\chi_{ij}} c^{\dagger}_{j\sigma} c_{i\sigma} + U \sum_i \left(n_{i\uparrow} - \frac{1}{2}\right)\left(n_{i\downarrow} - \frac{1}{2}\right). \quad (1)$$

The noninteracting part is a tight-binding Hamiltonian on a square lattice with each plaquette threaded with half a flux quantum $\frac{1}{2}\Phi_0 = \frac{1}{2}\frac{hc}{e}$ [27,28]. Here $c^\dagger_{i\sigma}$ and $c_{i\sigma}$ are the creation and annihilation operators at site $\mathbf{r}_i$ with spin $\sigma = \uparrow, \downarrow$; the hopping amplitude between the nearest-neighbor sites i and j is t_{ij}. χ_{ij} is the Peierls phase, given by $\chi_{i,i+\hat{x}} = 0, \chi_{i,i+\hat{y}} = \pi i_x$ in the Landau gauge. The resulting hopping pattern is shown in Fig. 1(a). When t_{ij} is uniform, the lattice has a two-site unit cell (with labels A, B) and in reciprocal space, with the reduced Brillouin zone ($|k_x| \leqslant \pi/2, |k_y| \leqslant \pi$), the noninteracting Hamiltonian can be written as

$$H_0 = \sum_{\mathbf{k}\sigma} \psi^\dagger_{\mathbf{k}\sigma} \mathcal{H}_0(\mathbf{k}) \psi_{\mathbf{k}\sigma}, \quad \psi_{\mathbf{k}\sigma} = \begin{pmatrix} c_{A\sigma} & c_{B\sigma} \end{pmatrix}^T,$$
$$\mathcal{H}_0(\mathbf{k}) = \begin{pmatrix} -2t\cos k_y & +2t\cos k_x \\ +2t\cos k_x & +2t\cos k_y \end{pmatrix}. \tag{2}$$

The energy spectrum $E_\mathbf{k} = \pm\sqrt{4t^2(\cos^2 k_x + \cos^2 k_y)}$ describes a semimetal with two inequivalent Dirac points at $\mathbf{K}_\pm = (\pi/2, \pm\pi/2)$.

Introducing t_{ij} with the pattern shown in Fig. 1(b), the unit cell is also doubled along the y direction. The two Dirac points are folded to the same point $(\pi/2, \pi/2)$ in the reduced Brillouin zone. The Hamiltonian in momentum space becomes

$$H_0 = \sum_{\mathbf{k}\sigma} \psi^\dagger_{\mathbf{k}\sigma} \mathcal{H}_0(\mathbf{k}) \psi_{\mathbf{k}\sigma},$$
$$\psi_{\mathbf{k}\sigma} = (c_{A\sigma} \quad c_{B\sigma} \quad c_{C\sigma} \quad c_{D\sigma})^T,$$
$$\mathcal{H}_0(\mathbf{k}) = \begin{pmatrix} 0 & 2t_+\cos k_x & -2t_-\cos k_y & 0 \\ & 0 & 0 & 2t_+\cos k_y \\ & & 0 & 2t_-\cos k_x \\ & & & 0 \end{pmatrix}, \tag{3}$$

where the lower triangle is filled so that the matrix is Hermitian. Now the energy spectrum is $E_\mathbf{k} = \pm 2t_\pm\sqrt{\cos^2 k_x + \cos^2 k_y}$ with $t_\pm = (1 \pm \alpha)t_0$ and $t_+ = 1$ defines the energy scale. We obtain "birefringent" fermionic Dirac species with distinct velocities $2t_\pm$.

When treated within mean-field theory, AF order is represented by an additional real-space term $H_{\mathrm{AF}} = m\sum_i (-1)^l (c^\dagger_{i\uparrow}c_{i\uparrow} - c^\dagger_{i\downarrow}c_{i\downarrow})$, where $(-1)^l = +1(-1)$ if site l is on the two sublattices of the bipartite square lattice. The spectrum $E'_\mathbf{k} = \pm 2t_\pm\sqrt{\cos^2 k_x + \cos^2 k_y + m^2}$ is immediately gapped.

We will, instead, analyze the behavior within an exact treatment of the correlations by simulating the π-flux Hubbard model Eq. (1) using the DQMC method [29–32]. To characterize the magnetic properties, we measure the staggered structure factor $S(\pi,\pi) = \frac{1}{N}\sum_{i,j}(-1)^l \langle \mathbf{S}_i \cdot \mathbf{S}_j \rangle$. A physical quantity of central interest is the sublattice magnetization, which is given by $M^2 = S(\pi,\pi)/N$. We also employ the stochastic series expansion (SSE) QMC method with directed loop update to simulate the corresponding Heisenberg model of the Hamiltonian Eq. (1) in the strong coupling limit [33]. The SSE QMC is performed using the ALPS libraries [34].

III. DECREASED CRITICAL INTERACTION AT THE SEMIMETAL TO AF INSULATOR TRANSITION

Figure 2 shows S_{AF} on a $N = 8 \times 8$ lattice for different U as a function of α. At the π-flux lattice point ($\alpha = 0$), it is known that long-ranged antiferromagnetic order (LRAFO) exists when U exceeds $U_c = 5.65 \pm 0.05$ [18]. In the $\alpha = 1$ limit, the geometry is the Lieb lattice, where LRAFO (or, more precisely, ferrimagnetic order) exists for all $U > 0$. The behavior of S_{AF} is qualitatively similar for different values of the interaction strength U: S_{AF} first increases at small α; quantum antiferromagnetism is enhanced. However, after reaching a maximum at intermediate $0 < \alpha < 1$, the structure factor falls off. Intuitively, the final decrease in spin-spin correlations, as $\alpha \to 1$ might be associated with the bonds, are being increasingly weakened, and indeed are finally completely depleted from the lattice at $\alpha = 1$.

To gain additional insight into the behavior of S_{AF}, it is useful to examine the equal-time *real space* spin-spin correlation function $c(\mathbf{r}) = \langle (n_{j+\mathbf{r}\uparrow} - n_{j+\mathbf{r}\downarrow})(n_{j\uparrow} - n_{j\downarrow}) \rangle$. $c(\mathbf{r})$ is spin-rotation invariant, and in our simulations we average the z correlation above over all three directions to provide an improved estimator [35]. Figure 3 shows the spin-spin correlation function for $U = 3$ at $\alpha = 0.5, 0.7, 0.9$ on a 16×16 lattice. The origin is placed on the A site at (0,0), and $\mathbf{r}$ runs along a triangle path. The path in Fig. 3(a) contains A, B, D sites. The absolute values of $c(\mathbf{r})$ grow monotonically as α is increased, reaching the Lieb lattice limit at $\alpha = 1$. Their signs are consistent with antiferromagnetic order. $\alpha = 0.5$ is close to the critical point, thus the value of the correlation at large distance is relatively small at the temperature considered. On the other hand, the correlation length has become comparable to the system size for the cases of $\alpha = 0.7, 0.9$. $c(\mathbf{r})$ has a robust persistence at large distance, suggesting the existence of the LRAFO.

Along the path in Fig. 3(b), which only contains C sites, the correlations are always negative since the sites are on the opposite sublattice from the origin. The trend in their amplitude with increasing α is initially the same as that of Fig. 3(a): the correlations grow in size with α. Crucially, however, after reaching a maximum at $\alpha \sim 0.7$ they rapidly decline. This is then the real-space origin of the nonmonotonicity of S_{AF} with α.

The behavior of S_{AF} is suggestive of the fact that LRAFO may develop at a decreased critical interaction in the presence of bond weakening in going from the π-flux lattice to the Lieb lattice. We use finite size scaling on lattices of sizes $L = 8, 12, 16$ to analyze quantitatively the position of the critical point in the thermodynamic limit. We calculate the structure factor as a function of β, which is shown in Fig. 4(a). At low β, the correlation length is short, and S_{AF} is independent of L. At large β, S_{AF} first grows with L, then tends to a constant. Therefore we use $\beta = 20$ to guarantee that the system is in the ground state.

The square of the order parameter is given by S_{AF}/N in the limit $1/L \to 0$, for example, Fig. 4(b) shows such extrapolation at $\alpha = 0.4$. These extrapolated values are shown in Fig. 5. As a function of $t_- = v/2$ (v is the velocity of the outer Dirac cone), the critical interaction strength is continuously decreased to zero. The quantum phase transition between

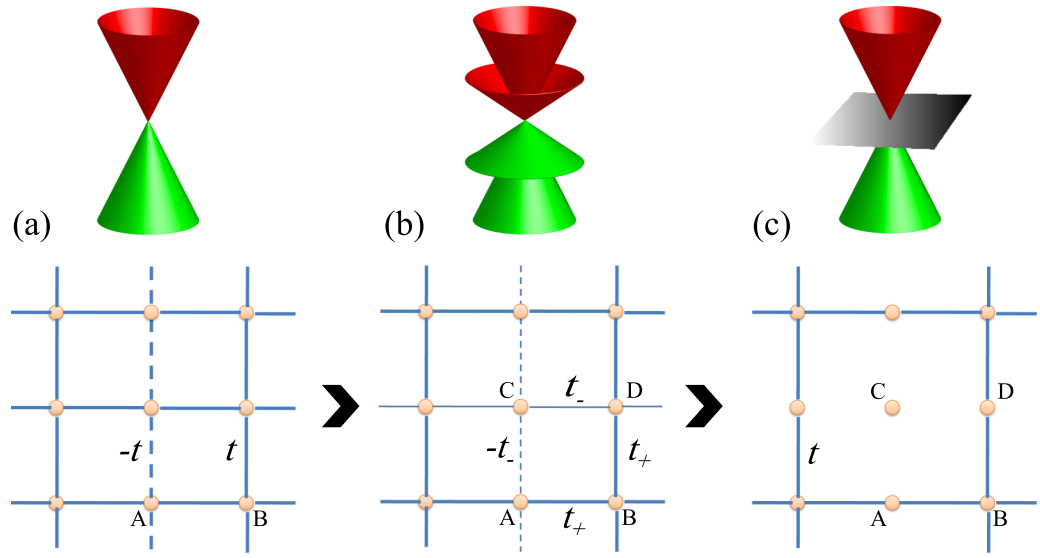

FIG. 1. The energy spectra and lattice geometries considered in this paper. (a) The π-flux lattice has two identical single Dirac cones. The solid (dashed) lines represent positive (negative) hoppings. (b) The unit cell is doubled by an alternation of the hoppings $t_\pm = (1 \pm \alpha)t_0$, and, as a result, there are two Dirac cones with different velocities. (c) In the limit $\alpha = 1$, one of the four sites in one unit cell is completely depleted since the hoppings to it, $t_- = 0$. The resulting geometry is a Lieb lattice ($\frac{1}{4}$ depleted square lattice).

the semimetal and antiferromagnetic insulator is continuous. For the π-flux Hubbard model, the critical exponents have been calculated in Refs. [18,19]. It is natural that the phase transition at different anisotropic factors should belong to the same universality class. With the data at hand, we estimate the critical exponents $\beta = 0.65(0.17)$ for $\alpha = 0.4$. It is pointed out in Ref. [18] that the critical exponents for the π-flux model have to be determined with very large lattice sites. However, our estimation roughly confirms that the critical exponents do not depend on α within statistical error. We also perform a mean-field analysis and the critical interactions are underestimated. The same situation happens for interacting Dirac fermions on honeycomb lattice, where the mean field gives $U_c = 2.23$ [36], compared to $U_c = 3.87$ from DQMC [17].

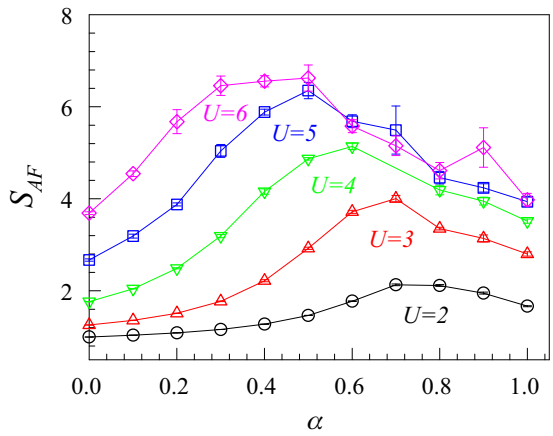

FIG. 2. The AF structure factor $S_{\rm AF}$ as a function of α for different U at $\beta = 10$. The linear size $L = 8$ and the number of sites $N = 64$. Data were acquired from 10 simulations of 1000 equilibration and 10 000 measurement sweeps for each α.

Recent studies of the honeycomb and π-flux Hubbard models show that the critical interactions are different. But by rescaling U_c with the geometric average of the velocities, it is obtained $\frac{U_c}{\sqrt{v_x v_y}} = 4.4(4.2)$ for the honeycomb Hubbard model (π-flux Hubbard model). Considering the difference of the bandwidths, the scaled critical interactions can be thought to be equal, thus it suggests that the velocities of the Dirac fermions are the main contribution to the renormalization of U_c [18,19]. However, the velocities in these models are not tunable if one wants to keep the bandwidths fixed. In contrast, in the system studied here, the velocities of one species of Dirac

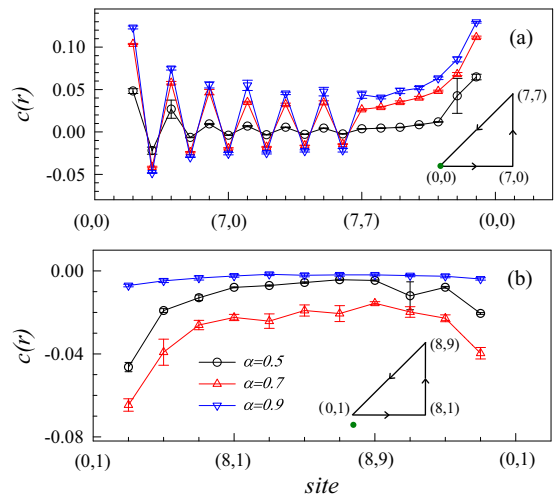

FIG. 3. The equal time spin-spin correlation function $c(\mathbf{r})$ on a 16×16 lattice at $\beta = 10$. Data are shown for various α at $U = 3$, including $\alpha = 0.7$ which has the largest $S_{\rm AF}$. (a) $c(\mathbf{r})$ between A site at (0,0) and A, B, D sites along the triangular path on the lattice shown in the inset. (b) $c(\mathbf{r})$ between A site at (0,0) and C sites on the path of the inset. The green dot denotes the A site at the origin (0,0).

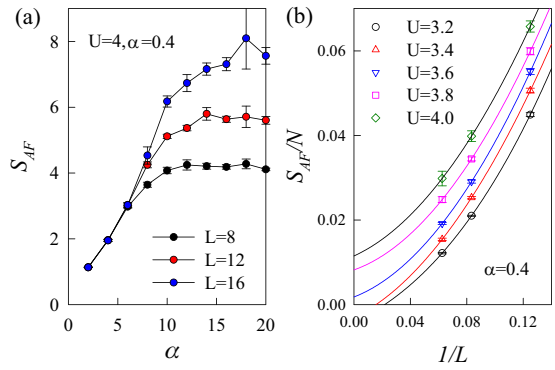

FIG. 4. (a) The antiferromagnetic structure as a function of β and different lattice sizes L at $U/t = 4$. (b) Extrapolation of $S_{\rm AF}/N$ at different U/t values. Here the anisotropic factor $\alpha = 0.4$.

fermions are continuously tuned, while the other species fixes the bandwidth. Thus one is able to make a definitive statement concerning the evolution of U_c measured in the meaningful limit of fixed bandwidth.

IV. 2D HEISENBERG MODEL WITH WEAKENED BONDS

It is well known that the half-filled Hubbard model, which describes itinerant magnetism, maps onto the antiferromagnetic (localized spin-1/2) Heisenberg model

$$H = J \sum_{\langle i,j \rangle} \mathbf{S}_i \cdot \mathbf{S}_j \quad (J > 0), \tag{4}$$

as $U/t \to \infty$. The relation $J = 4t^2/U$ gives the exchange constant in terms of U and the hopping amplitude. The 2D square lattice Heisenberg model with uniform J has been studied intensely by means of various theoretical and numerical techniques. There is a general consensus that antiferromagnetic long-range order exists in the ground state [37]. We consider here the inhomogeneous variant corresponding to the Hamiltonian Eq. (1) describing two species of Dirac fermions,

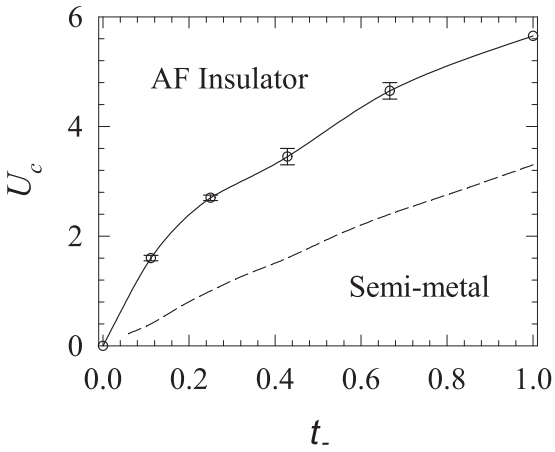

FIG. 5. The critical interaction U_c in the thermodynamic limit as a function t_- (the hopping amplitudes on the weakened bonds, which is $\frac{1-\alpha}{1+\alpha}$). The dashed line is from the mean-field theory. The velocity of the outer Dirac cone is $v = 2t_-$. The inverse temperature is $\beta = 20$.

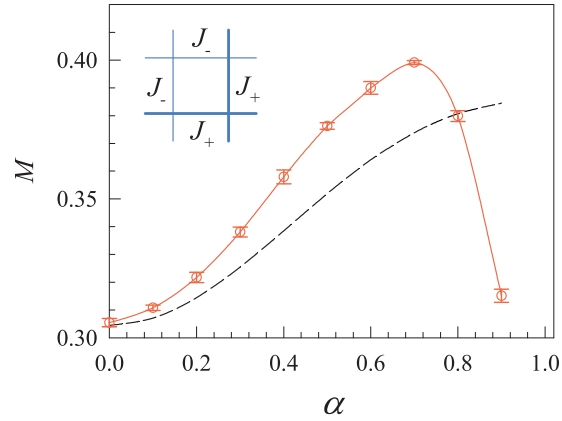

FIG. 6. The sublattice magnetization of the 2D spin-1/2 Heisenberg model in the thermodynamic limit, as a function of the modulation strength α of the exchange constants. The inverse temperature is $\beta = 100$, which is low enough to acquire the ground state [38]. The dashed line is from the linear spin-wave theory (see Appendix B for the details). The inset shows the four-site unit cell with the modulated coupling $J_\pm$. In the simulations, $J_+ = 1$ is fixed as the energy scale, and $J_- = (1-\alpha)^2/(1+\alpha)^2$ on the weakened bonds.

in which the antiferromagnetic coupling is modulated with $J_\pm = (1 \pm \alpha)^2 J$. (See inset to Fig. 6.)

M is calculated on $L \times L$ lattices with L up to 48, and is extrapolated to the thermodynamic limit using fits to polynomials in $1/L$. Figure 6 shows the extrapolated values as a function of α. At $\alpha = 0$ we recover the 2D Heisenberg model, obtaining $M = 0.3055 \pm 0.0015$, which is consistent with previous QMC results [39,40]. As the bonds are weakened, the antiferromagnetic correlations are enhanced. The data shows a peak with a maximum $M = 0.399$ at about $\alpha = 0.7$. The order parameter increases to about 80% of the classical limit, emphasizing the reduction of quantum fluctuations. At this maximum, the coupling $J_- = 0.0311$. Beyond $\alpha \sim 0.7$, M decreases quickly. In the limit $\alpha = 1$, where $J_- = 0$, the square lattice is depleted to Lieb lattice, and the extrapolated value $M = 0.3842$. We also calculate the sublattice magnetization using the linear spin-wave theory (see Fig. 6). In most cases, the magnetization M is underestimated and the nonmonotonic dependence on α cannot be obtained.

The enhancement of the sublattice magnetization can also be explained by analyzing explicitly the details of the real-space spin-spin correlation function, similar to the fermionic case shown in Fig. 3. Figure 7 shows $c(\mathbf{l})$ ($\mathbf{l}$ is the maximum distance on the finite lattice) in the different channels. It is interesting to see that the correlation with C site first rises rapidly and then dives, in contrast to the slow rise or the small change in the correlations between A, B, D sites. Thus the behavior of the sublattice magnetization is dominated by the correlations with the depleted C sites.

There are other ways to arrange weakened couplings, generating anisotropic, dimerized, and plaquette Heisenberg models, which have been much studied due to the relevance to the pinning effects of the electronic liquid crystal in the underdoped cuprate superconductor $YBa_2Cu_3O_{6.45}$, or being important examples featuring a quantum phase transition [41–44]. However, in these cases, the sublattice magnetization

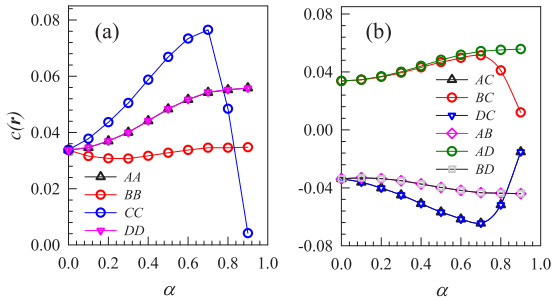

FIG. 7. The spin-spin correlation function $c(\mathbf{r})$ between the two most distant points on a 48×48 lattice in the different channels. AA and DD channels in (a) are degenerate, and $AC(AB)$ and $DC(BD)$ channels in (b) are degenerate.

decreases monotonically as the bonds are weakened. The quantum antiferromagnetic enhancement found here is intriguing since it does not correspond to the qualitative trends in this past work. Besides our explicit explanation by analyzing spin-spin correlation function, another fact should be noted that in the limit cases the above spatially anisotropic models becomes a 1D Heisenberg model, or isolated dimers and plaquettes, which have no long-ranged antiferromagnetism order.

V. CONCLUSIONS

The interaction-driven semimetal to antiferromagnetic insulator transition of two coupled species of Dirac fermions, realized by depleting the π-flux lattice to the Lieb lattice, was studied using the DQMC method. During the process of increasing the modulation of the hopping, the quantum antiferromagnetism is enhanced, resulting in a decreased critical interaction U_c at the quantum phase transition. A related phenomenon of increased sublattice magnetization in the corresponding Heisenberg model was also confirmed. The Hamiltonian studied provides a clean, idealized system in which to explore the effect of velocity on the critical interaction strength for magnetic ordering and MITs of Dirac fermions.

Moreover, ultracold atoms in optical lattices provide a platform to implement this system. Very recently, the 2D Fermi-Hubbard model has been realized in a series of experiments and spin correlations displaying antiferromagnetic behavior have been observed directly with Bragg scattering [45] and fermionic microscopes [46–49]. In addition, a scheme based on resonant modulations was developed to engineer synthetic gauge fields and a constant flux per plaquette throughout the optical lattice [50]. This offers the possibility of "building" the modified π-flux Hubbard model whose physics was explored here, and verifying experimentally our key findings.

The enhancement of magnetic order with inhomogeneous hopping patterns which we find is, in fact, an intriguing feature of a number of strong correlation phenomena. It has been proposed, for example, that an "optimal inhomogeneity" exists for d-wave superconductivity in a Hubbard model which builds a full 2D lattice from 2×2 plaquettes serving as binding centers for d-wave pairs [51–54]. However, a considerable degree of discussion has arisen from different results obtained within complementary analytic and numeric approaches, both for the magnetic and pairing responses [55–57]. We have shown that the idea of optimal inhomogeneity extends further to Dirac fermions, and also proposed a way to tune the inhomogeneity so that the velocity can be used to adjust the position of the quantum critical point between paramagnetic metal and antiferromagnetic insulating ground state phases.

ACKNOWLEDGMENTS

The authors thank R. Mondaini, T. Mendes-Santos, R. R. P. Singh, and Shengyuan A. Yang for helpful discussions. H.G. acknowledges support from China Scholarship Council and NSFC Grant No. 11774019. L.W. is supported by the Ministry of Science and Technology of China under the Grant No. 2016YFA0300603. R.T.S. was supported by DOE Grant No. DE-SC0014671.

APPENDIX A: MEAN-FIELD APPROXIMATION OF THE HUBBARD MODEL

In the mean-field approximation, the interaction term in Eq. (1) is decoupled as

$$n_{i\uparrow}n_{i\downarrow} = \langle n_{i\downarrow}\rangle n_{i\uparrow} + \langle n_{i\uparrow}\rangle n_{i\downarrow} - \langle n_{i\downarrow}\rangle\langle n_{i\uparrow}\rangle. \tag{A1}$$

To incorporate the antiferromagnetism order, we write

$$\begin{aligned}\langle n_{i\uparrow,\alpha}\rangle &= \tfrac{1}{2} + \rho_\alpha, \langle n_{i\downarrow,\alpha}\rangle = \tfrac{1}{2} - \rho_\alpha, (\alpha = A, D),\\ \langle n_{i\uparrow,\alpha}\rangle &= \tfrac{1}{2} - \rho_\alpha, \langle n_{i\downarrow,\alpha}\rangle = \tfrac{1}{2} + \rho_\alpha, (\alpha = B, C).\end{aligned} \tag{A2}$$

Then the Hubbard term becomes

$$\begin{aligned}&U\sum_i n_{i\uparrow}n_{i\downarrow}\\ &= E_0 + \sum_{i\in A}(-\rho_A n_{i\uparrow} + \rho_A n_{i\downarrow}) + \sum_{i\in B}(\rho_B n_{i\uparrow} - \rho_B n_{i\downarrow})\\ &\quad + \sum_{i\in D}(-\rho_D n_{i\uparrow} + \rho_D n_{i\downarrow}) + \sum_{i\in C}(\rho_C n_{i\uparrow} - \rho_C n_{i\downarrow}),\end{aligned} \tag{A3}$$

where $E_0 = \frac{1}{4}NU + \frac{NU}{4}(\rho_A^2 + \rho_B^2 + \rho_C^2 + \rho_D^2)$ (N is the total number of the sites). The Hamiltonian matrix in the momentum space reads

$$\mathcal{H}_{\mathrm{MF}}^{\uparrow(\downarrow)}(\mathbf{k}) = \begin{pmatrix} \mp\rho_A & 2t_+\cos k_x & -2t_-\cos k_y & 0\\ & \pm\rho_B & 0 & 2t_+\cos k_y\\ & & \pm\rho_C & 2t_-\cos k_x\\ & & & \mp\rho_D \end{pmatrix}. \tag{A4}$$

The dispersion $E_{\mathbf{k},\sigma}$ can be obtained by diagonalizing the above Hamiltonian. However, the analytical result is complex, and we do not show the result here. Then we may calculate the free energy at zero temperature

$$F = \sum_{\mathbf{k},\sigma} E_{\mathbf{k},\sigma} + E_0, \tag{A5}$$

where the summation is over the two lower branches, which correspond to half-filling. The ground state is obtained by minimizing F with respect to the order parameters $\rho_\alpha(\alpha = A, B, C, D)$. This yields a set of self-consistent equations and can be calculated numerically.

APPENDIX B: LINEAR SPIN-WAVE THEORY OF THE HEISENBERG MODEL

Using Holstein-Primakoff transformation, the spin operators are expressed in term of bosonic creation and annihilation operators. The square lattice is a bipartite one. The transformation on one sublattice ($\alpha = A, D$) is defined as

$$\begin{aligned} S^+_{a,i} &= (\sqrt{2S - a^\dagger_{i,\alpha} a_{i,\alpha}})a_{i,\alpha}, \\ S^-_{a,i} &= a^\dagger_{i,\alpha}(\sqrt{2S - a^\dagger_{i,\alpha} a_{i,\alpha}}), \\ S^z_{a,i} &= S - a^\dagger_{i,\alpha} a_{i,\alpha}. \end{aligned} \tag{B1}$$

On the other sublattice ($\alpha = B, C$), the spin is in the opposite direction for the antiferromagnetism order. Thus the spin operators are defined as

$$\begin{aligned} S^+_{b,i} &= a^\dagger_{i,\alpha}(\sqrt{2S - a^\dagger_{i,\alpha} a_{i,\alpha}}), \\ S^-_{b,i} &= (\sqrt{2S - a^\dagger_{i,\alpha} a_{i,\alpha}})a_{i,\alpha}, \\ S^z_{b,i} &= a^\dagger_{i,\alpha} a_{i,\alpha} - S. \end{aligned} \tag{B2}$$

Expanding the square root in Eqs. (B1) and (B2) in powers of $1/S$, the zeroth order terms are kept in the linear spin-wave theory. Then the spin-wave Hamiltonian of Eq. (4) is directly obtained as

$$\begin{aligned} H =& -4N_t J_+ S(S+1) - 4N_t J_- S(S+1) \\ &+ \sum_{i=1}^{N_t} [2J_+ S(a_{i,A} a^\dagger_{i,A} + a^\dagger_{i,B} a_{i,B}) \\ &+2J_- S(a_{i,A} a^\dagger_{i,A} + a^\dagger_{i,C} a_{i,C}) \\ &+2J_+ S(a_{i,D} a^\dagger_{i,D} + a^\dagger_{i,B} a_{i,B}) \\ &+2J_- S(a_{i,D} a^\dagger_{i,D} + a^\dagger_{i,C} a_{i,C}) \\ &+J_+ S(a_{i,A} a_{i\pm x,B} + a^\dagger_{i,A} a^\dagger_{i\pm x,B}) \\ &+J_- S(a_{i,A} a_{i\pm y,C} + a^\dagger_{i,A} a^\dagger_{i\pm y,C}) \\ &+J_+ S(a_{i,D} a_{i\pm y,B} + a^\dagger_{i,D} a^\dagger_{i\pm y,B}) \\ &+J_- S(a_{i,D} a_{i\pm x,C} + a^\dagger_{i,D} a^\dagger_{i\pm x,C})], \end{aligned} \tag{B3}$$

where N_t is the number of unit cells. Perform a Fourier transformation, the above Hamiltonian writes as $H = \sum_{\mathbf{k}} \Psi^\dagger_{\mathbf{k}} \mathcal{H}(\mathbf{k}) \Psi_{\mathbf{k}}$, where $\Psi_{\mathbf{k}} = (a_{\mathbf{k},A}, a_{\mathbf{k},D}, a^\dagger_{-\mathbf{k},B}, a^\dagger_{-\mathbf{k},C})^T$ is the basis and $\mathcal{H}(\mathbf{k})$ is the following matrix:

$$\begin{aligned} &\begin{pmatrix} J_+ + J_- & 0 & J_+ \cos k_x & J_- \cos k_y \\ 0 & J_+ + J_- & J_+ \cos k_y & J_- \cos k_x \\ J_+ \cos k_x & J_+ \cos k_y & 2J_+ & 0 \\ J_- \cos k_y & J_- \cos k_x & 0 & 2J_- \end{pmatrix} \\ &= \begin{pmatrix} \mathbf{K^a} & \Delta \\ \Delta^T & \mathbf{K}^b \end{pmatrix}. \end{aligned} \tag{B4}$$

$\mathcal{H}(\mathbf{k})$ is also known as grand dynamical matrix and can be diagonalized by a Bogoliubov transformation

$$\begin{pmatrix} \alpha_{k,1} \\ \alpha_{k,2} \\ \beta^\dagger_{k,1} \\ \beta^\dagger_{k,2} \end{pmatrix} = \begin{pmatrix} u_{11} & u_{12} & v_{11} & v_{12} \\ u_{21} & u_{22} & v_{21} & v_{22} \\ w^*_{11} & w^*_{12} & x^*_{11} & x^*_{12} \\ w^*_{21} & w^*_{22} & x^*_{21} & x^*_{22} \end{pmatrix} \begin{pmatrix} a_{k,A} \\ a_{k,D} \\ a^\dagger_{-\mathbf{k},B} \\ a^\dagger_{-\mathbf{k},C} \end{pmatrix}. \tag{B5}$$

The coefficient is determined by the following non-Hermitian eigenproblem:

$$\begin{pmatrix} \mathbf{K^a} & -\Delta \\ \Delta^T & -\mathbf{K}^b \end{pmatrix} \begin{pmatrix} \bar{u} \\ \bar{v} \end{pmatrix} = \omega_n \begin{pmatrix} \bar{u} \\ \bar{v} \end{pmatrix}, \tag{B6}$$

$$\begin{pmatrix} \mathbf{K^a} & -\Delta \\ \Delta^T & -\mathbf{K}^b \end{pmatrix} \begin{pmatrix} \bar{w}^* \\ \bar{x}^* \end{pmatrix} = -\omega'_n \begin{pmatrix} \bar{w}^* \\ \bar{x}^* \end{pmatrix}, \tag{B7}$$

where $\omega_n, \omega'_n > 0$. The staggered magnetization is then given by

$$\begin{aligned} M &= \frac{1}{N} \sum_{i=1}^{N_t} \sum_{\alpha=A,B,C,D} \langle S^z_{i,\alpha} \rangle \\ &= S - \frac{1}{N} \sum_{\mathbf{k}} \sum_{\alpha=A,B,C,D} \langle a^\dagger_{\mathbf{k},\alpha} a_{\mathbf{k},\alpha} \rangle, \end{aligned} \tag{B8}$$

which can be calculated using the coefficients from the inverse transformation of Eq. (B5).

[1] A. H. Castro Neto, F. Guinea, N. M. R. Peres, K. S. Novoselov, and A. K. Geim, Rev. Mod. Phys. **81**, 109 (2009).
[2] J. Alicea, Rep. Prog. Phys. **75**, 076501 (2012).
[3] S. R. Elliott and M. Franz, Rev. Mod. Phys. **87**, 137 (2015).
[4] N. Armitage, E. Mele, and A. Vishwanath, Rev. Mod. Phys. **90**, 15001 (2018).
[5] B. Bradlyn, J. Cano, Z. Wang, M. G. Vergniory, C. Felser, R. J. Cava, and B. A. Bernevig, Science **353**, aaf5037 (2016).
[6] I. C. Fulga and A. Stern, Phys. Rev. B **95**, 241116 (2017).
[7] M. Ezawa, Phys. Rev. B **94**, 195205 (2016).
[8] R. A. Vicencio, C. Cantillano, L. Morales-Inostroza, B. Real, C. Mejía-Cortés, S. Weimann, A. Szameit, and M. I. Molina, Phys. Rev. Lett. **114**, 245503 (2015).
[9] S. Mukherjee, A. Spracklen, D. Choudhury, N. Goldman, P. Öhberg, E. Andersson, and R. R. Thomson, Phys. Rev. Lett. **114**, 245504 (2015).
[10] M. R. Slot, T. S. Gardenier, P. H. Jacobse, G. C. P. van Miert, S. N. Kempkes, S. J. M. Zevenhuizen, C. M. Smith, D. Vanmaekelbergh, and I. Swart, Nat. Phys. **13**, 672 (2017).
[11] R. Drost, T. Ojanen, A. Harju, and P. Liljeroth, Nat. Phys. **13**, 668 (2017).
[12] F. Kalff, M. Rebergen, E. Fahrenfort, J. Girovsky, R. Toskovic, J. Lado, J. Fernández-Rossier, and A. Otte, Nat. Nanotechnol. **11**, 926 (2016).
[13] B. Dóra, J. Kailasvuori, and R. Moessner, Phys. Rev. B **84**, 195422 (2011).

[14] Z. Lan, N. Goldman, A. Bermudez, W. Lu, and P. Öhberg, Phys. Rev. B **84**, 165115 (2011).

[15] Z. Lan, A. Celi, W. Lu, P. Öhberg, and M. Lewenstein, Phys. Rev. Lett. **107**, 253001 (2011).

[16] Z. Y. Meng, T. C. Lang, S. Wessel, F. F. Assaad, and A. Muramatsu, Nature (London) **464**, 847 (2010).

[17] S. Sorella, Y. Otsuka, and S. Yunoki, Sci. Rep. **2**, 992 (2012).

[18] Y. Otsuka, S. Yunoki, and S. Sorella, Phys. Rev. X **6**, 011029 (2016).

[19] F. Parisen Toldin, M. Hohenadler, F. F. Assaad, and I. F. Herbut, Phys. Rev. B **91**, 165108 (2015).

[20] L. Wang, P. Corboz, and M. Troyer, New J. Phys. **16**, 103008 (2014).

[21] Z.-X. Li, Y.-F. Jiang, and H. Yao, New J. Phys. **17**, 085003 (2015).

[22] E. H. Lieb, Phys. Rev. Lett. **62**, 1927 (1989).

[23] N. C. Costa, T. Mendes-Santos, T. Paiva, R. R. d. Santos, and R. T. Scalettar, Phys. Rev. B **94**, 155107 (2016).

[24] M. P. Kennett, N. Komeilizadeh, K. Kaveh, and P. M. Smith, Phys. Rev. A **83**, 053636 (2011).

[25] B. Roy, P. M. Smith, and M. P. Kennett, Phys. Rev. B **85**, 235119 (2012).

[26] N. Komeilizadeh and M. P. Kennett, Phys. Rev. B **90**, 045131 (2014).

[27] Y. Jia, H. Guo, Z. Chen, S.-Q. Shen, and S. Feng, Phys. Rev. B **88**, 075101 (2013).

[28] G. Rosenberg, B. Seradjeh, C. Weeks, and M. Franz, Phys. Rev. B **79**, 205102 (2009).

[29] R. Blankenbecler, D. J. Scalapino, and R. L. Sugar, Phys. Rev. D **24**, 2278 (1981).

[30] S. R. White, D. J. Scalapino, R. L. Sugar, E. Y. Loh, J. E. Gubernatis, and R. T. Scalettar, Phys. Rev. B **40**, 506 (1989).

[31] E. Y. Loh, J. E. Gubernatis, R. T. Scalettar, S. R. White, D. J. Scalapino, and R. L. Sugar, Phys. Rev. B **41**, 9301 (1990).

[32] J. E. Hirsch, Phys. Rev. B **31**, 4403 (1985).

[33] O. F. Syljuåsen and A. W. Sandvik, Phys. Rev. E **66**, 046701 (2002).

[34] B. Bauer, L. D. Carr, H. G. Evertz, A. Feiguin, J. Freire, S. Fuchs, L. Gamper, J. Gukelberger, E. Gull, S. Guertler, A. Hehn, R. Igarashi, S. V. Isakov, D. Koop, P. N. Ma, P. Mates, H. Matsuo, O. Parcollet, G. Pawlowski, J. D. Picon, L. Pollet, E. Santos, V. W. Scarola, U. Schollwöck, C. Silva, B. Surer, S. Todo, S. Trebst, M. Troyer, M. L. Wall, P. Werner, and S. Wessel, J. Stat. Mech.: Theor. Exp. (2011) P05001.

[35] C. N. Varney, C.-R. Lee, Z. J. Bai, S. Chiesa, M. Jarrell, and R. T. Scalettar, Phys. Rev. B **80**, 075116 (2009).

[36] S. Sorella and E. Tosatti, Europhys. Lett. **19**, 699 (1992).

[37] J. D. Reger and A. P. Young, Phys. Rev. B **37**, 5978 (1988).

[38] Here we use $\beta = 100$ for the Heisenberg model but only $\beta = 20$ for the Hubbard one. The reason is that one needs to go to lower temperature on larger lattices. For the Heisenberg case, we use the lattice size $L = 48$, thus the temperature needs to be colder to get the correlation length to reach the lattice size.

[39] A. W. Sandvik, Phys. Rev. B **56**, 11678 (1997).

[40] M. Calandra Buonaura and S. Sorella, Phys. Rev. B **57**, 11446 (1998).

[41] F.-J. Jiang, F. Kämpfer, and M. Nyfeler, Phys. Rev. B **80**, 033104 (2009).

[42] A. F. Albuquerque, M. Troyer, and J. Oitmaa, Phys. Rev. B **78**, 132402 (2008).

[43] J. Sirker, A. Klümper, and K. Hamacher, Phys. Rev. B **65**, 134409 (2002).

[44] S. Wenzel and W. Janke, Phys. Rev. B **79**, 014410 (2009).

[45] R. Hart, P. Duarte, T. Yang, X. Liu, T. Paiva, E. Khatami, R. Scalettar, N. Trivedi, D. Huse, and R. Hulet, Nature (London) **519**, 211 (2015).

[46] L. W. Cheuk, M. A. Nichols, K. R. Lawrence, M. Okan, H. Zhang, E. Khatami, N. Trivedi, T. Paiva, M. Rigol, and M. W. Zwierlein, Science **353**, 1260 (2016).

[47] M. F. Parsons, A. Mazurenko, C. S. Chiu, G. Ji, D. Greif, and M. Greiner, Science **353**, 1253 (2016).

[48] J. H. Drewes, L. A. Miller, E. Cocchi, C. F. Chan, N. Wurz, M. Gall, D. Pertot, F. Brennecke, and M. Köhl, Phys. Rev. Lett. **118**, 170401 (2017).

[49] A. Mazurenko, C. S. Chiu, G. Ji, M. F. Parsons, M. Kanász-Nagy, R. Schmidt, F. Grusdt, E. Demler, D. Greif, and M. Greiner, Nature (London) **545**, 462 (2017).

[50] N. Goldman, J. Budich, and P. Zoller, Nat. Phys. **12**, 639 (2016).

[51] H. Yao, W.-F. Tsai, and S. A. Kivelson, Phys. Rev. B **76**, 161104 (2007).

[52] S. Baruch and D. Orgad, Phys. Rev. B **82**, 134537 (2010).

[53] R. M. Fye, D. J. Scalapino, and R. T. Scalettar, Phys. Rev. B **46**, 8667 (1992).

[54] P. M. Smith and M. P. Kennett, Phys. Rev. B **88**, 214518 (2013).

[55] D. G. S. P. Doluweera, A. Macridin, T. A. Maier, M. Jarrell, and T. Pruschke, Phys. Rev. B **78**, 020504 (2008).

[56] T. A. Maier, M. Jarrell, and D. J. Scalapino, Phys. Rev. B **74**, 094513 (2006).

[57] S. Chakraborty, D. Sénéchal, and A.-M. S. Tremblay, Phys. Rev. B **84**, 054545 (2011).